A shallow water type model to describe the dynamic of thin partially wetting films

J. LALLEMENT^a, P. VILLEDIEU^a, P. TRONTIN^a , C. LAURENT^a

a. Onera - The French Aerospace Lab (Toulouse) - ONERA - F-31055 Toulouse, France,
julien.lallement@onera.fr

Abstract :

The objective of this work is to model the motion and the instabilities of partially wetting thin liquid films to derive models for the formation of wet and dry surfaces. The main idea of the work consists in reformulating the shallow water equations by introducing a disjoining pressure to model the effects of a partial wetting. Emphasis is put on the numerical treatment of the capillary forces, especially those acting in the vicinity of the contact line, since they can strongly influence the development of instabilities. We use an extended system that consists in reducing the order of the shallow water system by adding one evolution equation. This model is suited for numerical purposes since the surface tension term only involves second order derivatives instead of third order derivatives in the classical shallow water systems with two equations. A conservative formulation of the system and the associated energy are derived. One-dimensional numerical simulations using a first order implicit finite volume scheme have been performed. Droplet's stationnary shape, spreading length and time on an horizontal substrate is well recovered for all contact angle. Moreover, based on a linear stability analysis, unstable dewetting regimes of an infinite film of uniform thickness are identified and simulated.

Key words : shallow water, runoff, capillarity, triple line, deicing

1 Introduction

The motion and stability of liquid thin films and droplets which wet a solid substrate are present in a lot of natural and industrial processes and have been the object of a lot of research studies for several decades [3, 7, 6]. In the context of deicing, when a thermal protection system is activated, the supercooled water droplets impacting an aircraft surface don't freeze instantaneously and can coalesce and form a thin liquid film as a result of aerodynamic forces. Experimental studies show that this liquid film isn't always stable and can split into rivulets that may refreeze on unprotected surfaces [35]. The modeling of rivulet flows and the accurate prediction of wet and dry surfaces is important since it has a direct influence on the wall heat and mass fluxes such as evaporation or exchanges with the boundary layer.

The classical model for modeling thin fluids flow are the Navier-Stokes equations based on Newton's second law to the fluid, that are to be coupled with appropriate initial and boundary conditions. It is possible to reduce the N-S equations by using the property of thin films that the ratio of the film thickness h and any in-plane length-scale is small (long-wave approximation), and averaging the equations over the fluid thickness. The reduction of N-S equations can lead to one single non-linear fourth order partial

differential equation for h also called lubrication equation [1], or a third order system of two equations for h and the flow rate q also called shallow water equations by adding a closure assumptions on the normal film velocity profile which can be justified either by asymptotic analysis or by empirical arguments [2]. These models take account of viscosity, capillary, and gravitational effects and are generally preferred to N-S equations since they give satisfying results with a significant reduction of computational time. However, these classical models don't consider the molecular forces between interfaces acting in the triple line and thus are limited to totally wetting, which means that a liquid film on a solid substrate won't adopt an equilibrium state but will spread indefinitely. In addition, film rupture due to possibly destabilizing molecular forces is not included [19, 21, 30, 31, 32, 33, 34].

To take into account molecular forces and model the effects of partial wetting, an additional pressure term introduced by Frumkin and Derjaguin [8, 9, 10, 11], called disjoining pressure, is generally included into lubrication equation. The disjoining pressure $\Pi^d(h)$ is an additional force per unit area, arising from the interaction between two interfaces separated by a distance h. In the thin liquid films, these two interfaces are the solid-liquid and the liquid-air interface. The disjoining pressure $\Pi^d(h)$ can consist of several interactions, the best understood are van der Waals, electrical double layer and polar interactions, each acting on its scale and each influencing the value of the contact angle. The disjoining pressure can also be seen as a more general concept to regularize the discontinuous forces which come into play at the contact line. Following this interpretation, alternative phenomenological models for the disjoining pressure have appeared in the literature : a diffuse interface model by Thiele & Pomeau that is based on exponential functions [18, 20], power-law expressions [13, 14, 16], or combinations of power-law and exponential expressions have also been used [15, 17]. These models make the approximation of a disjoining pressure between two unbounded parallel interfaces. In reality, and especially near the contact line, the interfaces are generally neither flat nor unbounded. Dai [22] and Hocking [23] incorporated the gradient and curvature of the liquid film into the expression of the disjoining pressure.

In general hydrodynamic studies, the usual boundary condition used for a fluid moving on a solid substrate is a no-slip condition : the fluid velocity vanishes in contact with the substrate. This boundary condition is well-suited for macroscopic scale, but it is not for smaller scales especially where the two interfaces meet at the contact line [24, 25]. This problem is known as the contact line paradox. The incompatibility between the usual no-slip condition, where the moving liquid meets the substrate, and the boundary condition on the liquid-gas interface, leads to a non-integrable force singularity and doesn't allow a liquid to move on a perfectly dry region since it should dissipate an infinite amount of energy. A number of solutions to fix this problem have been proposed. A first solution is the add of a slip length that allows the fluid to slip at the boundary [5, 26, 27]. Some authors rather use a disjoining pressure combining long-range repulsive and short-range attractive forces leading to an energetically stable film thickness h_* [13, 14, 15, 16, 17]. Introduction of such a disjoining pressure avoids the use of the slip model because the precursor layer present everywhere on the substrate acts as a slip coefficient, but this method has a drawback : from a physical point of view, precursor films are usually not encountered under partially wetting conditions.

In this paper we present the first step (2D case) of a more general work which aims at simulating motion and transverse instabilities of a partially wetting thin liquid film on a solide substrate. Following some ideas from the literature, the contact line forces are taken into account thanks to a disjoining pressure term. A suitable expression of this term has been chosen to ensure the partial wettability of the substrate with a true dry region even at the microscopic scale (no precursor film) [4]. As far as the contact line paradox is concerned, the approach based on the introduction of a slip lenght has been used. But contrary

to what is usually done in the literature for thin film modelling, we do not use here the lubrication equation. This one is replaced by an extended shallow water model wich is written in a conservative form and which is formally equivalent to the lubrication equation in the limit of negligible inertial effects. The big advantage of using this new formulation lies in the fact that the new model corresponds to a second order differential system whereas the lubrication equation is a fourth order partial differential equation. For this reason, the new proposed formulation is much more suited to finite volume discretization methods. This property remains valid in 3D and will allow to use arbitrary surface meshes in future work.

The rest of the paper is organized as follows. In section 2, we present how to derive the extended shallow water model and how it is related to the classically used lubrication equation. The model for the disjoining pressure is introduced as well. Section 3 is devoted to the linear stability analysis of the model solutions. It is shown that a planar liquid film is unstable (dewetting phenomena) as soon as its thickness is lower than a threshold which is of the same order as the cutting length used in the definition of the disjoining pressure. The numerical discretization method is presented in section 4, section 5 is devoted to numerical validation tests. The final section gives a status of the present work and future outlook.

2 Derivation of the extended shallow water model

Mathematical model

The mathematical problem is formulated by considering an incompressible liquid film on an inclined plane which makes an angle β to horizontal. The x and z axes are respectively parallel and perpendicular to the substrate, the liquid surface thus corresponds to $z = h(x,t)$. Liquid film motion is typically described under the framework of lubrication equation, which has for expression :

$$\frac{\partial h}{\partial t} + \frac{\partial (h\overline{u})}{\partial x} = 0 \qquad (1)$$

$$h\overline{u} = -m(h) \left(\frac{\partial}{\partial x} \left[g_n h + \frac{\gamma}{\rho} K - \Pi^d(h) \right] - g_t \right) \qquad (2)$$

with h the fluid thickness, $\overline{u}$ the mean fluid velocity (that we will write u by omitted the "overline" symbol for simplicity), and $m(h) = h^2(h+b)/3\nu$ the mobility factor due to the assumed Poiseuille flow, with b a slip length preventing viscous stress divergence for vanishing film thicknesses [27]. $g_n h$ represents the hydrostatic pressure, γK the Laplace pressure, with K the free surface curvature and γ the liquid/vapor surface tension, and $\Pi^d(h) = -\partial G^d/\partial h$ a disjoining pressure arising from partial wetting effects, with G^d the disjoining energy. g_n and g_t are respectively the acceleration of gravity g projected onto the x and z axis due to plane inclination, ν is the cinematic viscosity, and ρ the fluid density.

The lubrication equation has the disadvantage to involve fourth order spatial derivatives, since K involves second order derivatives, which is difficult to discretize. It is possible to formally derive (1) from a more general third order system, also called shallow water equation system, which reads :

$$\frac{\partial h}{\partial t} + \frac{\partial q}{\partial x} = 0 \qquad (3)$$

$$\frac{\partial q}{\partial t} + \frac{\partial \left(h\overline{u^2} \right)}{\partial x} + h \frac{\partial}{\partial x} \left[g_n h + \frac{\gamma}{\rho} K - \Pi^d(h) \right] = hg_t + \tau_w \qquad (4)$$

with $q = hu$ the flow rate integrated over the fluid thickness, $\overline{u^2}$ the mean squared velocity, and

$\tau_w(h) = -\frac{3\,\nu\,u}{h+b}$ the friction between the fluid and the wall. One can easily verify that in the assumption of negligible inertia ($\frac{\partial q}{\partial t}$ and $\frac{\partial(hu^2)}{\partial x} \ll 1$), the system is equivalent to (1).

In the study of thin film flows on solid substrates, the free surface curvature is generally approximated by $K \simeq -\frac{\partial^2 h}{\partial x^2}$. These approximations are strictly applicable for problems with vanishing free surface slopes, which is not necessarily true in the vicinity of the contact line. We adopt here a generalization of the classical shallow water equations by taking the full expression of the curvature $K = -\frac{\partial}{\partial x}\left[\left(\frac{\partial h}{\partial x}\right)/\sqrt{1+\left(\frac{\partial h}{\partial x}\right)^2}\right]$. We approximate that the mean squared velocity $\overline{u^2} \approx u^2$ assuming that inertial effects are small, without entirely neglecting it. To allow a finite volume discretization, it is more convenient to write the shallow water system $\{(3),(4)\}$ under the equivalent conservative form :

$$\frac{\partial h}{\partial t} + \frac{\partial q}{\partial x} = 0 \tag{5}$$

$$\frac{\partial q}{\partial t} + \frac{\partial\left(hu^2\right)}{\partial x} + \frac{\partial}{\partial x}\Pi\left(h,\partial h/\partial x,q\right) = \frac{\partial}{\partial x}B\left(h,\partial h/\partial x\right) + hg_t + \tau_w \tag{6}$$

with the forces per unit length Π and B in equation (6) given by :

$$\Pi = g_n \frac{h^2}{2} + \frac{1}{\rho}\left(-\frac{\gamma}{\sqrt{1+\left(\frac{\partial h}{\partial x}\right)^2}} + \left(h\frac{\partial G^d}{\partial h} - G^d\right)\right) \tag{7}$$

where the first term is the hydrostatic pressure force, the second represents the capillary tension which correspond to the liquid/vapor surface tension parallel to the liquid free surface projected onto the x axis, and the last term is the disjoining force acting at the contact line.

$$B = \frac{\gamma}{\rho}\,h\,\frac{\partial}{\partial x}\left(\frac{\left(\frac{\partial h}{\partial x}\right)}{\sqrt{1+\left(\frac{\partial h}{\partial x}\right)^2}}\right) = -\frac{\gamma}{\rho}\,h\,K \tag{8}$$

which represents the pressure jump across the liquid/vapor interface caused by its curvature, also called Laplace pressure [4].

The term $\left(\frac{\partial B}{\partial x}\right)$ on the right side of the equation (6) is third order in space, which is still hard to discretize, particularly on non-structured mesh for future three-dimensional works. One solution is to consider like Noble & Vila [36] a new unknown $p = \left(\frac{\partial h}{\partial x}\right)$ that will be computed independently with a new equation. By spatially deriving equation (5), we obtain the transport equation for p :

$$\frac{\partial p}{\partial t} + \frac{\partial\left(u\,p\right)}{\partial x} = -\frac{\partial}{\partial x}\left(h\,\frac{\partial u}{\partial x}\right) \tag{9}$$

Adding this equation to (5) and (6) reduces by an order in space the system of equation, which results in the following second order system of three equations for h, p and q :

$$\begin{cases} \frac{\partial h}{\partial t} + \frac{\partial q}{\partial x} = 0 \\ \frac{\partial p}{\partial t} + \frac{\partial(up)}{\partial x} = -\frac{\partial}{\partial x}\left(h\frac{\partial u}{\partial x}\right) \\ \frac{\partial q}{\partial t} + \frac{\partial(uq)}{\partial x} + \frac{\partial}{\partial x}\left[g_n\frac{h^2}{2} + \frac{1}{\rho}\left(-\frac{\gamma}{\sqrt{1+p^2}} + \left(h\frac{\partial G^d}{\partial h} - G^d\right)\right)\right] = \frac{\partial}{\partial x}\left[\frac{\gamma}{\rho}\,h\,\frac{\partial}{\partial x}\left(\frac{p}{\sqrt{1+p^2}}\right)\right] + hg_t + \tau_w \end{cases} \tag{10}$$

One can introduce the energy density per unit length of the film :

$$e\left(h, p, q\right) = \frac{hu^2}{2} + g_n \frac{h^2}{2} + \frac{1}{\rho}\left(\gamma \ \sqrt{1+p^2} + \gamma_{sl} + G^d(h)\right) \tag{11}$$

which is composed of a gravitational energy represented by $g_n \frac{h^2}{2}$, of a capillary energy proportional to the area of the liquid surface represented by $\gamma \ \sqrt{1+p^2}$, of the energy between the liquid and the solid substrate equal to the surface tension γ_{sl} between these two phases, and of the disjoining energy $G^d(h)$ associated to partially wetting effects.

Using (5), (6), (9) and (11), it is possible to establish the following energy balance equation :

$$\frac{\partial e}{\partial t} + \frac{\partial\left(u\,e\right)}{\partial x} + \frac{\partial\left(u\,\Pi\right)}{\partial x} = \frac{\partial}{\partial x}\left({}^t\underline{\varphi}.\underline{\underline{A}}.\frac{\partial\underline{\varphi}}{\partial x}\right) + u\left(hg_t + \tau_w\right) \tag{12}$$

with $\underline{\varphi} = \left(\partial e/\partial h, \partial e/\partial p, \partial e/\partial q\right)$ a thermodynamic variable vector, and $\underline{\underline{A}}$ an anti-symmetric matrix. Assuming no plane inclination ($g_t = 0$), equation (12) is conservative with a dissipation source term (it can be shown easily that $u\,\tau_w \leq 0$). Consequently, the total energy of the film $E = \int\left[e\left(h, p, q\right)\right]\,\mathrm{d}x$ is a non-increasing function of time, which is a proof of the thermodynamic consistency of the model.

Disjoining energy model

Using an exact expression of disjoining energy G^d to model partially wetting effects at the molecular scale would require highly refined mesh and consequently high computational costs. We will rather use a phenomenological model assuming that the disjoining energy $G^d(h)$ is a function depending of the thickness h, which ensures a continuously transition from the capillary energy of a dry substrate ($e = \gamma_{sv}$) to the energy of a wet substrate ($e = \gamma + \gamma_{sl}$), with γ_{sv} the solid/vapor surface tension.
A lot of models to regularize the disjoining energy can be found in the literature, we adopt here a simple exponential expression : $G^d(h) = S\,exp\left(-h/h_*\right)$, where $S = \gamma_{sv} - \gamma_{sl} - \gamma$ is known in the literature as the spreading coefficient. It expresses the energy difference between a dry and a wet substrate, and is linked to the static contact angle $S = \gamma\left(cos\left(\theta_s\right) - 1\right)$ [12].

The plot of the capillary energy density per unit length $e(h) = \gamma_{sl} + \gamma + G^d(h)$ in figure 1b shows that this choice of disjoining energy, plotted in figure 1a, ensures a concave connection between the energy of a dry and a wet substrate, which is caracteristic of a partial wetting situation [4].

(a) Sketch of the disjoining energy $G^d(h)$ (b) Sketch of the energy $e(h) = \gamma_{sl} + \gamma + G^d(h)$
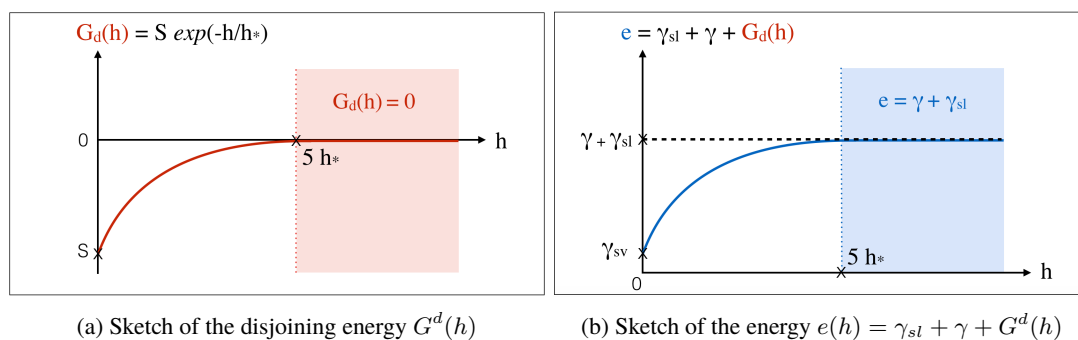
FIGURE 1 – Sketch of the disjoining energy $G^d(h)$ and the capillary energy density $e(h)$ of a flat film

Here the disjoining model has a single adjustable parameter h_*, which corresponds to the characteristic length scale of the exponential function. From a physical point of view, it is supposed to represent the

typical range of the microscopic forces which are in play in the vicinity of the contact line. But in our case, for numerical purposes, the value of this parameter will be chosen as a function of the mesh size (as will be shown later in Section 5) in order to smooth the effect of these forces without modifying the macroscopic behavior of the film (contact angle, apparent contact line velocity).

3   Linear stability analysis

We want to study the linear stability (LSA) of a planar liquid film in function of the modelling of wetting properties, which are the disjoining parameter h_* and the static contact angle θ_s. To study the linear stability of a film of uniform thickness h_o on a horizontal plane, we use a Fourier mode decomposition of the perturbation by setting $h = h_o + \varepsilon\, h_1\, exp\,(ikx + \omega t)$ and $u = \varepsilon\, u_1\, exp\,(ikx + \omega t)$, with $\varepsilon \ll 1$ the perturbation amplitude, $k = 2\pi/\lambda$ the wavenumber, and $\omega = \omega_r + i\,\omega_i$ the (real or complex) growth rate. Linearizing the equations (5) and (6) in $\varepsilon\, h_1$ and $\varepsilon\, u_1$ leads to the expression of the growth rate ω :

$$\omega = \omega_r = -\frac{h_o^2\,(h_o + b)}{3\mu}\, k^2\left[g + \frac{1}{\rho}\left(\frac{\partial^2 G^d}{\partial h^2}\right)_{(h=h_o)} + \frac{\gamma}{\rho}\,k^2\right] \tag{13}$$

One can notice that the growth rate is strongly linked to the energy density per unit length of the liquid, since $\left(\frac{\partial^2 e}{\partial h^2}\right) = g + \frac{1}{\rho}\left(\frac{\partial^2 G^d}{\partial h^2}\right)$. So the sign of $\left(\frac{\partial^2 e}{\partial h^2}\right)_{(h=h_o)}$ will determine the linear stability of the film. If $\left(\frac{\partial^2 e}{\partial h^2}\right) > 0$, the growth rate $\omega < 0$ and the film is linearly stable. If $\left(\frac{\partial^2 e}{\partial h^2}\right) < 0$, the growth rate $\omega > 0$ and the film is linearly unstable stable for all wave number in the range $0 < k < \sqrt{(\rho/\gamma)\,(\partial e/\partial h)_{(h=h_o)}}$. The wave number associated to the maximal growth rate can be calculated and is equal to :

$$k_m = \frac{1}{\sqrt{2}}\left[-\frac{\rho\,g}{\gamma} - \frac{1}{\gamma}\left(\frac{\partial^2 G^d}{\partial h^2}\right)_{(h=h_o)}\right] \tag{14}$$

The dewetting pattern of a linearly unstable liquid film will be predominantly piloted by the increasing amplitude of the wavelength $\lambda_m = 2\pi/k_m$ of maximal growth rate.

The limit of stability is found by finding the solutions of $\left(\frac{\partial^2 e}{\partial h^2}\right) = 0$ and results in the curves plotted in figure 2.
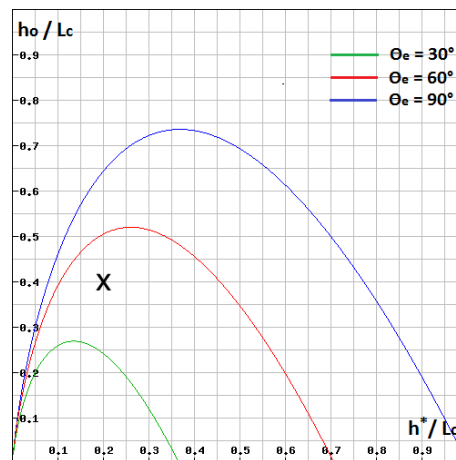

FIGURE 2 – Linearly unstable domain of a film of thickness h_o for different static contact angles θ_s. The linearly stable domain is above the curve, and the unstable one is below the curve. The thickness h_o and the parameter h_* are plotted in units of the capillary length $l_c = \sqrt{\gamma/\rho g}$. The cross corresponds to $(h_*/l_c\,,\,h_o/l_c) = (0.2\,,\,0.4)$.

We see that for sufficiently thick films, the film is linearly stable for all h_*. This is due to the fact that the range of the regularized forces $(= O(h_*))$ is too short to create interactions between the solid-liquid and the liquid-air interfaces. We can also observe that the film cannot be destabilized by inter-molecular forces for great h_* as a result of the stabilizing effect of gravity. The value of the contact angle θ_s strongly influence the stability domain since the range of instability decreases as the contact angle decreases, and completely vanishes for $\theta_s = 0°$, which is consistent with the fact that a totally wetting fluid is stable.

This linear stability analysis highlights a first mechanism of film rupture, called in the literature surface instability dewetting regime. This regime appears generally in the case of very thin films, which thicknesses, of the order of the nanometer, are close to the range of inter-molecular forces.

However, we remind that the model of disjoining energy used here with the exponential function results in a range of these forces equal to $O(h_*)$. If the parameter h_* is taken to big, instability dewetting regimes can appear even for macroscopic films. Taking the example of liquid water $(l_c = 2.7 \; mm)$ with a static contact angle $\theta_s = 60°$, we can see with the cross on figure 2 that if we take $h_* = 0.2 \, l_c$, a liquid film of thickness $h_o = 0.4 \, l_c = 1.08 \; mm$, well above the nanometer scale, is linearly unstable. Consequently, we will have to be careful with the choice of h_* to avoid generating non-physical instabilities.

4   Numerical methods

The system of equation to be solved (10) can be written in the matrix form :

$$\frac{\partial \underline{U}}{\partial t} + \frac{\partial (u \, \underline{U})}{\partial x} + \frac{\partial \underline{F}}{\partial x} = \frac{\partial \underline{B}}{\partial x} + \underline{S} \tag{15}$$

where $\underline{U} = \begin{pmatrix} h \\ p \\ q \end{pmatrix}$ is the conservative variable vector, $\underline{F} = \begin{pmatrix} 0 \\ 0 \\ \Pi \end{pmatrix}$ represents first order fluxes,

$\underline{B} = \begin{pmatrix} 0 \\ -h\frac{\partial u}{\partial x} \\ \frac{\gamma}{\rho} h \frac{\partial}{\partial x}\left(\frac{p}{\sqrt{1+p^2}}\right) \end{pmatrix}$ second order fluxes, and $\underline{S} = \begin{pmatrix} 0 \\ 0 \\ hg_t + \tau_w \end{pmatrix}$ source terms.

The implicit in time and first order in space discretization scheme that we used for the system (15) reads :

$$\Delta x_i \frac{U_i^{n+1} - U_i^n}{\Delta t} + \left((u\,\underline{U})_{i+1/2}^{n+1} - (u\,\underline{U})_{i-1/2}^{n+1}\right) + \left(\underline{F}_{i+1/2}^{n+1} - \underline{F}_{i-1/2}^{n+1}\right) = \left(\underline{B}_{i+1/2}^{n+1} - \underline{B}_{i-1/2}^{n+1}\right) + \underline{S}_i^{n+1} \tag{16}$$

where i is the cell number, Δx_i the cell size and Δt the time step.

The terms $\underline{F}_{i+1/2}^{n+1}$, $(u\,\underline{U})_{i-1/2}^{n+1}$, $\underline{B}_{i+1/2}^{n+1}$ are respectively an implicit discretization of the continuous fluxes $\underline{F}$, $(u\,\underline{U})$ and $\underline{B}$ between the cell i and $i+1$. The term $\underline{S}_i^{n+1}$ is an implicit discretization of the continuous source terms $\underline{S}$ in the cell i. The spatial discretizations are composed of the following difference approximations :

- a first order upwind scheme for the convective flux $(u\,\underline{U})_{i+1/2}$:

$$(u\,\underline{U})_{i+1/2} = max\left(u_{i+1/2} \,,\, 0\right) \underline{U_i} + min\left(u_{i+1/2} \,,\, 0\right) \underline{U_{i+1}} \tag{17}$$

$$u_{i+1/2} = \frac{1}{2}\left(u_i + u_{i+1}\right) \tag{18}$$

- a first order central difference approximation for the flux $F_{i+1/2} = \left(0 \ , \ 0 \ , \ \Pi_{i+1/2}\right)$ and $B_{i+1/2}$:

$$\Pi_{i+1/2} = \frac{1}{2}\left(\Pi_i + \Pi_{i+1}\right) \tag{19}$$

$$\underline{B_{i+1/2}} = \begin{pmatrix} 0 \\ -\frac{1}{2\Delta x_i}\left(h_i + h_{i+1}\right)\left(u_{i+1} - u_i\right) \\ \frac{1}{2\Delta x_i}\left(h_i + h_{i+1}\right)\frac{\gamma}{\rho}\left(\frac{p_{i+1}}{\sqrt{1+p_{i+1}^2}} - \frac{p_i}{\sqrt{1+p_i^2}}\right) \end{pmatrix} \tag{20}$$

- the source term $\underline{S_i}$ is written :

$$\underline{S_i} = \begin{pmatrix} 0 \\ 0 \\ h_i \, g_t + (\tau_w)_i \end{pmatrix} \tag{21}$$

It can be shown that this numerical scheme verifies a numerical counterpart of the continuous energy balance equation (12).

The spatial discretization used here only involves first order difference approximations, the jacobian matrix is then a block tridiagonal matrix, and can be thus efficiently stored and inverted using a Thomas algorithm. Finally, to ensure a numerical convergence of the solution, the system is solved using an iterative Newton method.

5 Results

In this section, we perform simulations using the proposed extended shallow water model with the numerical discretization presented in the previous section. As a first step, we will calibrate the model by analysing the dependence of a droplet profile at equilibrium on the parameter h_*, which allows to adjust the disjoining force in the vicinity of the contact line, and on the mesh size Δx. The objective is to determine the couple $(h_* \ , \ \Delta x)$ that allows to capture acurately first the wet surface, which is the principal criteria in the context of deicing applications, then the static contact angle θ_s and the shape of the equilibrium state. Then, we validate our model using different academical cases : the spreading of droplets under the influence of gravity and without gravity, the comparison between our model and the one with a small-slope approximation, and the simulation of dewetting regimes based on LSA.

To evaluate numerically the time dependent apparent contact angle θ, we won't measure exactly the tangent between the drop and the dry substrate, since the droplet will have a circular shape that transitions smoothly to $h = 0$ because of the regularized force at the contact line. Instead, we measure the tangent at the inflection point in the vicinity of the contact line to evaluate the apparent contact angle θ, as shown in figure 3.
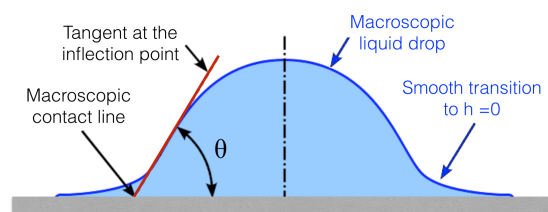

FIGURE 3 − Section of a droplet on a substrate. The angle θ represents the apparent contact angle measured in simulations.

5.1 Calibration of the model - Stationnary results of symetric spreading

We consider a parabolic profile for the film thickness at $t = 0\ s$ given by the following :

$$\forall x,\ h_i(x) = max\left[\sqrt{max\left[\frac{R_i^2}{sin\,(\theta_i)^2} - x^2\ ,\ 0\right]} - \frac{R_i}{tan\,(\theta_i)}\ ,\ 0\right] \qquad (22)$$

The value R_i is the initial radius and is chosen so that the total area of the liquid is equal to $A = \dfrac{2\,\theta_i - sin\,(2\theta_i)}{2\,sin\,(\theta_i)^2}R_i^2$ and the value θ_i is the initial contact angle. Here we choose $R_i = 10^{-2}\ m$ and $\theta_i = 80°$. The property of the liquid are those of water at ambiant temperature ($\gamma = 0.078\ N\ m^{-1}$, $\rho = 1000\ kg\ m^{-3}$, $\nu = 10^{-6}\ m^2\ s^{-1}$, $l_c = 2.7 \times 10^{-3}\ m$). The liquid is under the influence of gravity $\left(g = 9.81\ m\ s^{-2}\right)$ and is supposed to make a static angle $\theta_s = 60°$ with the substrate at equilibrium. The slip length b is fixed to $10^{-9}\ m$, its dynamic influence will be discussed further since the objective of these simulations is only to analyse steady state solutions.

The theoretical profile at equilibrium of a droplet of radius $R_i \gg l_c$ can be calculated numerically (see [3] for details), it has a puddle shape of thickness $h_{puddle} = 2\,l_c\,sin\,(\theta_s/2)$ far from the contact line, and has an approximate diameter $D_{puddle} \simeq A/h_{puddle}$, with A the area of the droplet. The relation giving h_{puddle} can be obtained with a force balance in the vicinity of the contact line represented in figure 4.
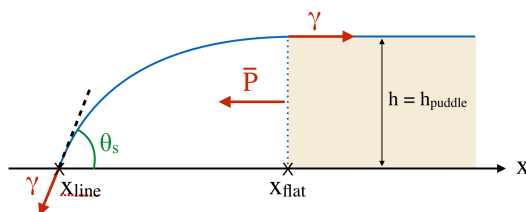

FIGURE 4 – Equilibrium of the forces acting on the edge of a puddle. $\overline{P} = \dfrac{\rho g h^2}{2}$ represents the hydrostatic pressure integrated along the film thickness.

5.1.1 Influence of the disjoining parameter h_*

We first investigate the dependence of the stationary profile on the disjoining parameter h_* at constant mesh size $\Delta x = 6 \times 10^{-5}\ m$. We suppose for now that numerical convergence is reached with this resolution, since the influence of the mesh size will be studied further.

Figure 5 shows the equilibrium profiles for various values of h_* close to the mesh size. We see that this choice of values leads to good results since the wet surface, the theoretical stationary shape (represented with small circles) and the static contact angle are all well recovered. In the case of $h_* = \Delta x/2$, the apparent contact angle reaches $53°$, which is close to $\theta_s = 60°$. These results can be explained by the fact that the regularized molecular forces are thinly spread and properly discretized.
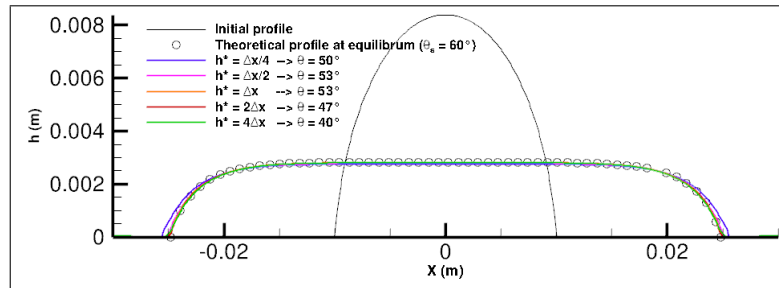
FIGURE 5 – Equilibrium profiles with $\theta_s = 60°$ for various values of h_* close to the mesh size Δx. For each case, the value of the calculated apparent contact angle θ is given in the legende.

The equilibrium profiles for h_* small compared to the mesh size are shown in figure 6. The wet surface and the theoretical stationary shape are not recovered for these values of h_*. The case $h_* = \Delta x/16$ leads to a relative error of 16 % on the wet surface. This is due to the fact that although the regularized forces in the contact line are thinly spread, they are poorly discretized.
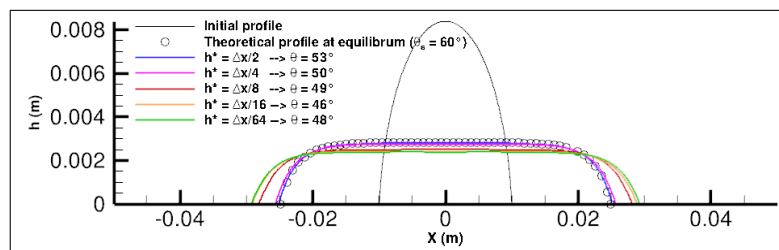

FIGURE 6 – Equilibrium profiles with $\theta_s = 60°$ for various values of h_* small compared to the mesh size Δx. For each case, the value of the calculated apparent contact angle θ is given in the legende.

If we assign high values to h_* compared to the mesh size or the liquid thickness h_{puddle} far from the triple line, the stationary profiles in figure 7 show that, if $h_* > h_{puddle}/10$, it is not possible to recover the wet surface, nor the theoretical stationary shape, nor the static contact angle. The relative error on the wet surface is 6% for $h_* = h_{puddle}/5$, and is 42% for $h_* = 2\,h_{puddle}/5$. The reason of these results is that too high values of h_* lead to a too spread force at the contact line. We can see that from $h_* = h_{puddle}/10$, the shape and more important the wet surface are in agreement with the theoretical solution, smaller values of h_* will only allow better values of contact angle : from $40°$ to $53°$ between $h_* = h_{puddle}/10$ and $h_* = \Delta x/2$.
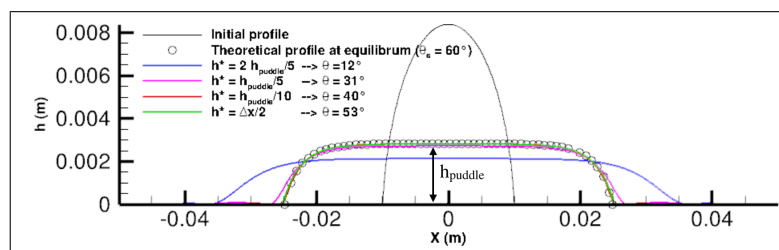

FIGURE 7 – Equilibrium profiles with $\theta_s = 60°$ for various values of h_* high compared to the mesh size Δx. The value $h_{puddle} (= 2\,l_c\,sin\,(\theta_s/2))$ corresponds to the liquid film thickness far from the triple line. For each case, the value of the calculated apparent contact angle θ is given in the legende.

These first simulations enabled us to determine a first condition on the parameter h_* to ensure good

stationnary results. If this parameter is kept within $O(\Delta x) \leq h_* \leq h_{puddle}/10$, the wet surface and the stationary shape are both well recovered, as desired for industrial applications.

5.1.2   Influence of the mesh size

We investigate now the dependence of the stationnary profile on the mesh size Δx at constant h_*. We choose $h_* = h_{puddle}/10$ since we have seen that this value gives satisfactory results. Figure 8 shows the equilibrium profiles for various values of mesh size compared to h_{puddle}. We can see that for every choice of mesh size, the wet surface is well recovered. In the case of mesh sizes greater than the film thickness, the error on the wet surface is only due to the coarsness of the mesh, the relative error is then limited to $\mid R_{puddle} - \Delta x \mid /R_{puddle}$. In the case of thin mesh sizes, convergence occurs from $\Delta x = h_{puddle}/10$, since thinnest mesh sizes only allow small improvement of contact angle : from $38°$ to $40°$ between $\Delta x = h_{puddle}/10$ and $\Delta x = h_{puddle}/50$, that is 5% improvement for a 5 times thinner mesh size.

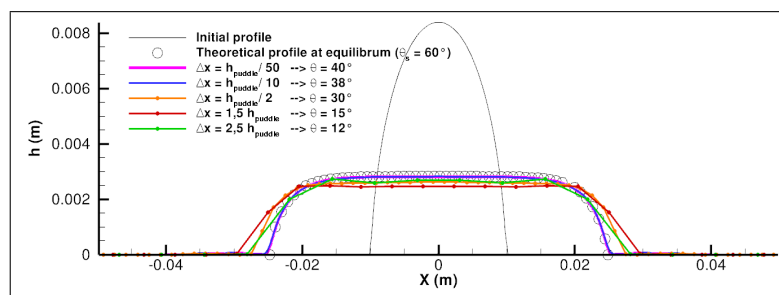FIGURE 8 – Equilibrium profiles with $\theta_s = 60°$ for various values of mesh size Δx. The value h_{puddle} $(= 2\, l_c\, sin\,(\theta_s/2))$ corresponds to the liquid film thickness far from the triple line. For each case, the value of the calculated apparent contact angle θ is given in the legende.

These analysis of the influence of the mesh size enabled us to determine two important informations about the choice of the parameter h_* and the mesh size Δx to ensure good stationnary results. First, for a given h_*, convergence is reached from $\Delta x = O(h_*)$ since this mesh size allows a good discretization of the regularized forces at the contact line. Then, for a coarse mesh ($\Delta x > h_{puddle}/10$), we just need to satisfy $h_* \leq h_{puddle}/10$ to recover the correct wet surface.

We can finally resume the conditions on h_* and Δx that allow to obtain good results in term of stationary shape and wet surface. In the case of academic simulations, like those realized in this section, on which thin mesh sizes can be used, we will take the parameter $h_* \leq h_o/10$, with h_o the order of magnitude of the encountered film thicknesses, and will take an adapted mesh size $\Delta x = O(h_*)$ that ensures a good discretization of the regularized force (at least 4 cells). In practice, we will always take the smallest value of h_* as possible in the limit of moderate computational costs (since $\Delta x = O(h_*)$), because we have seen in section 3 that if this value is set too high, unintended instabilities can appear.

In the context of industrial applications, simulations with coarse meshes ($\Delta x > h_o/10$) will mostly be encountered. We will give to h_* its real value, in the order of the nanometer, in order to avoid unintended instabilities. The value of this parameter doesn't matter as long as $h_* \leq h_o/10$, because the mesh is too coarse for correctly discretizing the regularized force at the contact line.

5.2   Validation of the model

5.2.1   Comparison with the small slope approximation

We want to verify that our extended shallow water model can recover a droplet stationary shape for every contact angles, even close to 90°, and that this model is an improvement of the usual one with the long wave approximation, in which the expressions (7), (8) and the expression of the disjoining energy $G^d(h)$ are approximated by :

$$\Pi \approx g_n \frac{h^2}{2} + \frac{1}{\rho} \left[- \left(1 - \frac{\gamma}{2} \left(\frac{\partial h}{\partial x} \right)^2 \right) + \left(h \frac{\partial G^d}{\partial h} - G^d \right) \right] \tag{23}$$

$$B \approx \frac{\gamma}{\rho} h \left(\frac{\partial^2 h}{\partial x^2} \right) \tag{24}$$

$$G^d(h) = \gamma \left(cos\left(\theta_s \right) - 1 \right) e^{-h/h_*} \approx -\gamma \left(\frac{\theta_s^2}{2} \right) e^{-h/h_*} \tag{25}$$

We still consider an initial parabolic profile of radius $R_i = 5 \times 10^{-3} \ m$ and making an initial angle θ_i with the substrate. The property of the liquid are those of water at ambiant temperature and the slip length b is fixed to $10^{-9} \ m$. The liquid is not under the influence of gravity $\left(g = 0 \ m \ s^{-2} \right)$ and is supposed to make a static angle θ_s with the substrate at equilibrium. The theoretical profile at equilibrium is then a parabolic profile of same area A given by :

$$\forall x, \ h_s(x) = max \left[\sqrt{max \left[\frac{R_s^2}{sin\left(\theta_s \right)^2} - x^2 , \ 0 \right]} - \frac{R_s}{tan\left(\theta_s \right)} , \ 0 \right] \tag{26}$$

$$R_s = sin\left(\theta_s \right) \sqrt{\frac{2 \ A}{2 \ \theta_s - sin\left(2 \ \theta_s \right)}} \tag{27}$$

Different simulations with various initial and static contact angles have been performed. The initial contact angle is taken $\theta_i = 45°$ for the simulations with $\theta_s = 15°$ and $\theta_s = 30°$, which represents a wetting configuration. We take $\theta_i = 30°$ for the simulations with $\theta_s = 45°$, $\theta_s = 60°$ and $\theta_s = 80°$, to simulate a dewetting configuration. For each simulations, we choose a mesh size Δx and a parameter h_* that respect the conditions of numerical convergence, which means that : $h_* < h_o/10$ and $\Delta x = O\left(h_* \right)$, where h_o represents the highest thickness of the stationary profile and is given by : $h_o = R_s \left(\frac{1}{sin\left(\theta_s \right)} - \frac{1}{tan\left(\theta_s \right)} \right)$.

Figure 9 shows the equilibrium profiles for various values of static contact angles θ_s from 15° to 80°. We can see that for contact angles less than 30° (figure 9a and 9b), the stationary profiles obtained with each models are hardly distinguishable and correspond to the theoretical profile at equilibrium. The differences are most significant for upper values of contact angles. Whereas the profiles obtained with the extended model correspond closely to the theoretical ones even for hydrophobic substrates $\left(\theta_s = 80° \right)$, the results with the "long wave" model differ from the awaited solutions. The relative error on the wet surface increases with the value of the static contact angle : from 6% for $\theta_s = 45°$ to 22% for $\theta_s = 80°$ (figure 9c to 9e).

(a) Equilibrium profiles with $\theta_s = 15°$. The $(h_*, \Delta x)$ values are $\left(2.5 \times 10^{-5}\ m, 2.5 \times 10^{-5}\ m\right)$.

(b) Equilibrium profiles with $\theta_s = 30°$. The $(h_*, \Delta x)$ values are $\left(2.5 \times 10^{-5}\ m, 2.5 \times 10^{-5}\ m\right)$.

(c) Equilibrium profiles with $\theta_s = 45°$. The $(h_*, \Delta x)$ values are $\left(3.75 \times 10^{-5}\ m, 2.5 \times 10^{-5}\ m\right)$.

(d) Equilibrium profiles with $\theta_s = 60°$. The $(h_*, \Delta x)$ values are $\left(3.75 \times 10^{-5}\ m, 2.5 \times 10^{-5}\ m\right)$.

(e) Equilibrium profiles with $\theta_s = 80°$. The $(h_*, \Delta x)$ values are $\left(7.5 \times 10^{-5}\ m, 1.25 \times 10^{-5}\ m\right)$.
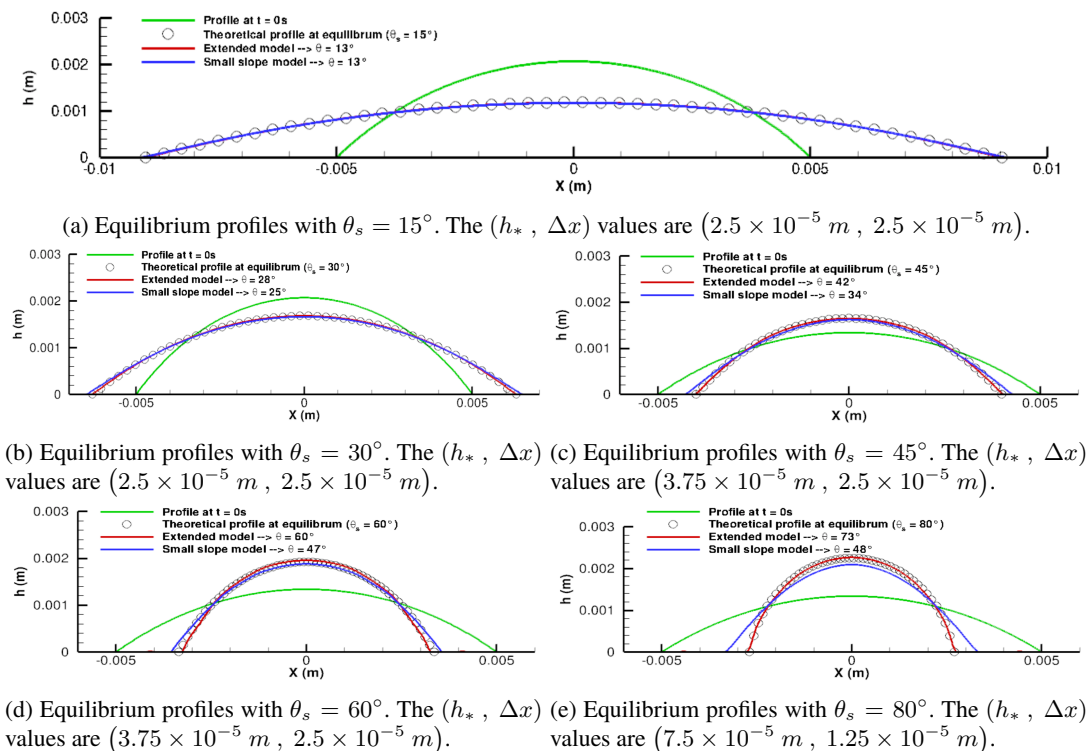
FIGURE 9 – Dependence of the droplet profile at equilibrium on the shallow water model. The red curve shows the profile obtained with the model proposed in this paper and the blue curve with the same model with small slope approximation. For each case, the value of the calculated apparent contact angle θ is given in the legende.

This study highlights the inability of the usual shallow water equations to simulate a droplet steady state on a substrate with high values of static contact angles, also called a hydrophobic substrate. The reason of this behavior is that the small slope approximation, as its name suggests, is limited to small slopes. Consequently, too high values of free surface slopes $(\partial h / \partial x)$ or values of contact angles θ_s break the applications limits of this model. The extended shallow water model presented here is then necessary to simulate droplet motion on both high and low-energy surfaces.

5.2.2 Dynamical results of axisymmetric spreading

As a first dynamic study of the model, we simulate the case of the symmetric spreading of a droplet on a horizontal substrate, and we verify that the time evolution of the central height of the droplet agrees with the power behavior referred as Tanner's law [28]. Considering a sufficiently small droplet, so that gravity can be neglected, and assuming small slopes at the free surface and thus a small contact angle, the decrease of the central height follows the law $h(x = 0, t) = K/t^{1/7}$ for a two-dimensional symmetric droplet. In addition to verifying this temporal law, we will also study the dependence of spreading time on the slip length b.

To respect the validity conditions of this law, the starting point is a parabolic profile of initial radius $R_i = 5 \times 10^{-4}\ m$ and making an angle $\theta_i = 50°$ with the substrate. The gravity is thus negligible since the initial radius is negligible with respect to the capillary length of the water $l_c \approx 2.7\ mm$. The static contact angle between the liquid and the substrate is $\theta_s = 4°$, the equilibrium state has thus a parabolic

shape of radius $R_f = sin\,(\theta_s)\,\sqrt{\frac{2A}{2\theta_s - sin(2\theta_s)}}$, with A the initial area of the droplet, and makes an angle $\theta_s = 4°$ with the substrate.

The parameter h_* is equal to 5×10^{-6} m, which respects the condition $h_* < h_o/10$, with h_o ($=$ 6.51×10^{-5} m) the highest thickness of the stationary profile, and we choose a mesh size $\Delta x = 4h_*$ ensuring a correct discretization of the force.

Figure 10 shows the central height $h(x = 0, t)$ plotted versus time for a partially wetting liquid ($\theta_s = 4°$), and also for a totally wetting liquid ($\theta_s = 0°$). We observe that the partially wetting case (curve in blue) agrees closely with the perfectly wetting case (curve in red) until the droplet has almost stabilized. These results are consistent with experimental studies conducted by Zosel [29]. He demonstrated that droplet spreading is independent of the nature of the substrate until close to stabilization. Using a logarithm scale, the two curves share before stabilization a same straight-line shape, due to a power-law behavior of expression : $h(0, t) = K/t^n$. Figure 10 represents the case of a slip length equal to 10^{-7} m, and the (K , n) parameters of the power-law are evaluated to $(7.64 \times 10^{-5}\, ,\, 0.137)$.

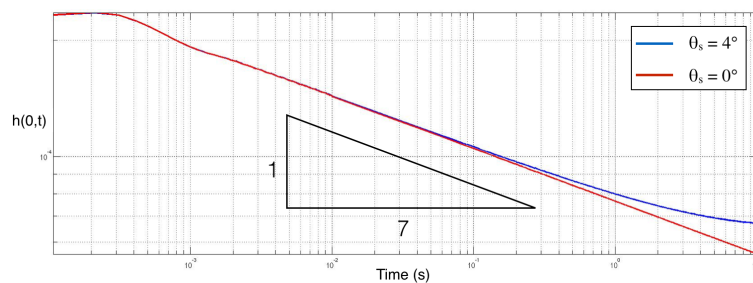FIGURE 10 – Comparison of the spreading time of the central height $h(0, t)$ between a partially ($\theta_s = 4°$) and a totally ($\theta_s = 0°$) wetting substrate, for a fixed value of slip length $b = 10^{-7}$ m. A logarithm scale is used.

The central height $h(x = 0, t)$ versus time for a partially wetting liquid ($\theta_s = 4°$) and for different values of slip length b is plotted in figure 11. We see that all cases exhibit a power-law behavior with approximately the same power exponent n close to $1/7$ as predicted by Tanner's law. For $b = 10^{-5}$ m, the parameters of the power-law are (K , n) $=$ $(6.58 \times 10^{-5}\, ,\, 0.15)$, for $b = 10^{-6}$ m we have $(7.32 \times 10^{-5}\, ,\, 0.144)$, for $b = 10^{-7}$ m we have $(7.65 \times 10^{-5}\, ,\, 0.137)$, and for $b = 10^{-8}$ m we have $(7.69 \times 10^{-5}\, ,\, 0.136)$. The slip length b only influences the value of K and will allow us to fit our model for unsteady motion simulations.
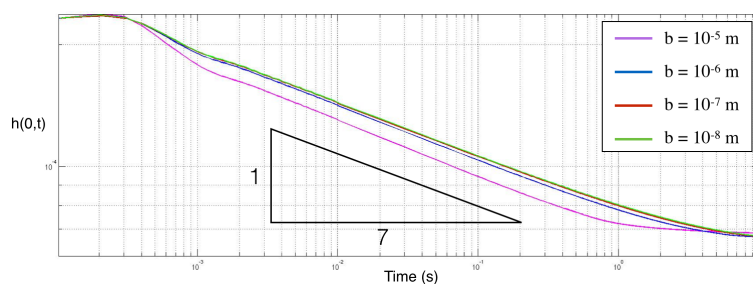

FIGURE 11 – Comparison of the spreading time of the central height $h(0, t)$ for different slip length b, for a partially wetting substrate ($\theta_s = 4°$). A logarithm scale is used.

These results indicate the existence of a self-similar solution to the problem appearing a short time after the start of the motion. In the case of partially wetting films, this self-similar solution is the same as for

a totally wetting film, since disjoining forces are negligible compared to the action of capillary pressure. The more the drop tends to flatten, the more the disjoining forces are dominant, and the spreading law of the partially wetting fluid changes since it progressively reaches its equilibrium state, whereas the totally wetting fluid continues to spread indefinitely.

5.2.3   Simulation of dewetting regimes of a film of uniform thickness

We consider an uniform film of thickness h_o and we want to study its linear stability in response of finite perturbations. To do so, we fix the value of the disjoining parameter $h_* (= 0.1 \, l_c)$, and choose different values of initial film thickness h_o from $0.01 \, l_c$ (in the linearly unstable domain) to $0.3 \, l_c$ (in the limit of the domain) as shown in figure 12. For the simulation, we init a liquid of thickness h_o for all $x \in [-R_i \, ; \, R_i]$ and a dry substrate ($h = 0$) elsewhere. The finite disturbance then consists of a pinch-off at the edges of the liquid film that will trigger the instabilities.

In the case of unstable dominated regimes, the finite disturbance will grow rapidly resulting in steady drops separated by a distance of $\lambda_m = 2\pi/k_m$, due to the dewetting piloted by the increasing amplitude of the wavelength λ_m of maximal growth rate. We will then verify that the model is able to simulate this regime, by comparing the number of steady drops obtained by numerical simulations N_{simu} with the number predicted by linear stability analysis $N_{LSA} = 2R_i/\lambda_m$.

FIGURE 12 – Stable and linearly unstable domains of an infinite flat film of thickness h_o for a static contact angle $\theta_s = 60°$. The thickness h_o and the parameter h_* are plotted in units of the capillary length l_c. The crosses correspond to the cases (h_*/l_c , h_o/l_c) studied in this section. A logarithm scale is used.

The property of the liquid are those of water at ambiant temperature, we consider the influence of gravity, we suppose a static angle $\theta_s = 60°$. The mesh size $\Delta x \left(= 2.7 \times 10^{-4} \, m\right)$ has been chosen so that the wavelength λ_m is correctly discretized for every case. The slip length b is fixed to $10^{-9} \, m$.

Figure 13 shows the initial and stationary profiles of liquid films characterized by their initial thickness h_o in the range $[0.01 \, l_c \, , \, 0.3 \, l_c]$. We can see that for every case simulated, the initial flat film of thickness h_o dewets into an array of stationnary drops. However, the number of drops strongly depends on the initial thickness, leading to smaller number of drops for thicker films. In the case of a small initial thickness (from $h_o = 0.01 \, l_c$ to $h_o = 0.1 \, l_c$), the stationary state agrees with the prediction of LSA since the number of resulting droplets N_{simu} is close to the number predicted N_{LSA} : for $h_o = 0.01 \, l_c$, we find $N_{simu} = 76$ and $N_{LSA} = 78$, for $h_o = 0.05 \, l_c$, we find $N_{simu} = 66$ and $N_{LSA} = 65$, and for $h_o = 0.1 \, l_c$, we find $N_{simu} = 53$ and $N_{LSA} = 50$.

For higher values of initial thicknesses, the number of resulting droplets becomes smaller than the number predicted by LSA. For $h_o = 0.2 \, l_c$, we find $N_{simu} = 23$ and $N_{LSA} = 28$ and for $h_o = 0.27 \, l_c$, we find $N_{simu} = 3$ and $N_{LSA} = 18$. This is due to the fact that for such values of h_o in the vicinity of the linearly unstable domain, we reach the limit of validity of the LSA since we are smoothly transitioning to the linearly stable domain and the dewetting regime is no more only piloted by the time increasing amplitude of the wavelength λ_m.
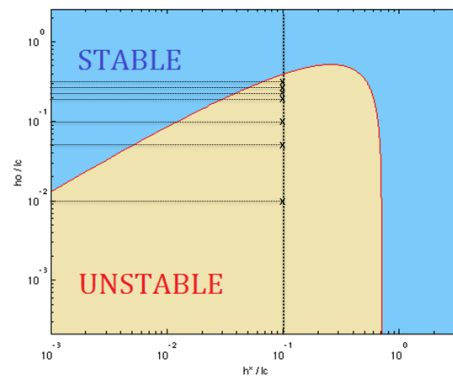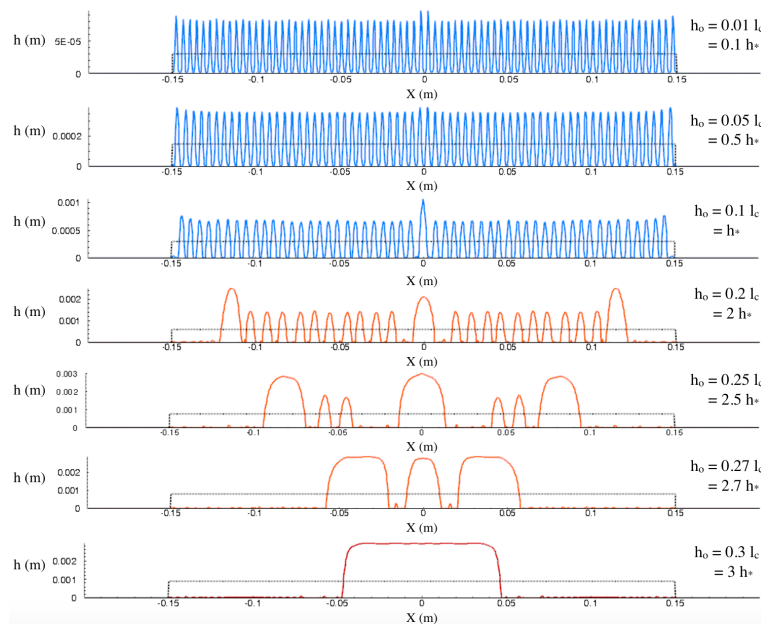
FIGURE 13 − Stationnary thickness profiles after different instability dewetting regimes depending on the initial value of the film thickness h_o. The dotted points represent the initial profile at $t = 0s$.

6 Discussion and conclusion

We have proposed an extended shallow water model which has the advantage to be only second order in space and takes into account capillary and inter-molecular forces without validity limits in terms of free surface slope and contact angle, contrary to classical lubrication models with long-wave approximations.

Based on a linear stability analysis, we have identified a regime that can lead to a film rupture : an instability dominated regime, where the evolution is piloted by the fastest film mode. This regime, generally appearing in the case of very thin films of thicknesses close to the range of inter-molecular forces, appears here for film thicknesses close to the parameter h_*, which acts as a regularization parameter to smooth the effect of these forces. This parameter must be carefully chosen, since too large values generate non-physical instabilities, and too small values require more computational costs because the mesh size must be of the same order as h_* to produce numerically accurate results.

The intention of this work was to derive a model that incorporates the most important features of the dynamics on scales much larger than the molecular scale. Two-dimensional simulations have demonstrated the feasibility of this model to simulate liquid motion on homogeneous substrates, and the results in term of steady state solution, dynamic spreading, and dewetting regime are all consistent with results of the literature.

The presented approach opens the door for simulation of liquid motion on a heterogeneous substrate, with add of dynamic contact angle and hysteresis effects, in order to simulate behaviors on a natural surface. The 3D extension of the method is also in progress, with the aim of a better understanding of rivulets flow formation.

Références

[1] Benney, D. J., Long waves on liquid films, J. Math. and Phys. 45, 150, 1966.

[2] V.Y. Shkadov, Wave Flow Regimes of a Thin Layer of Viscous Fluid subject to Gravity Izv. Akad. Nauk SSSR, Mekh. Zhidk. i Gaza 2, 1 , 43-51 (1970).

[3] P.G. de Gennes, Wetting : Statics and dynamics, Rev. Mod. Phys. 57, 827 (1985).

[4] P.G. de Gennes, F. Brochard-Wyart, D. Quéré, Capillarity and Wetting Phenomena : Drops, Bubbles, Pearls, Waves, Springer, New York (2004).

[5] E. B. Dussan V., The moving contact line : the slip boundary condition, J.Fluid Mech. 77, 665-684 (1976).

[6] E.B. Dussan V., On the spreading of liquids on solid surfaces : static and dynamic contact lines, Fluid Mech. 11, 371-400 (1979).

[7] J. H. Snoeijer, B. Andreotti, Moving Contact Lines : Scales, Regimes and Transitions, Annu. Rev. Fluid Mech.. 45, 269-92 (2013).

[8] Frumkin, A. N., On the phenomena of wetting and sticking of bubbles, Zh. Fiz. Khim. 12, 337 (1938).

[9] B. V. Deryaguin, Zh. Fiz. Khim. 14, 137 (1940).

[10] N. V. Churaev, Wetting films and wetting, Phys. Appl. 23, 975-987 (1988).

[11] N. V. Churaev, V.D. Sobolev, Prediction of contact angles on the basis of the Frumkin-Derjaguin approach, Advances in Colloid and Interface Science 61, 1-16 (1995).

[12] T. Young, An essay on the cohesion of fluids Philos. Trans. R. Soc. Lond. 95, 65 (1805)

[13] L.W. Schwart, D. Roux, J.J.Cooper-White, On the shapes of droplets that are sliding on a vertical wall, Physica D 209, 236-244 (2005).

[14] K.B. Glasner, Spreading of droplets under the influence of intermolecular forces, Physics of fluids 15, 7 (2003).

[15] A. Sharma, Relationship of thin film stability and morphology to macroscopic parameters of wetting in the apolar and polar systems, Langmuir 9, 861-869 (1993).

[16] A. Sharma, R. Khanna, Pattern Formation in Spontaneous Dewetting of Thin Apolar Films, Journal of Colloid and Interface science 195, 42-50 (1997).

[17] P. Beltrame, E. Knobloch, P. Hanggi, U. Thiele, Rayleigh and depinning instabilities of forces liquid ridges on heterogeneous substrates, Physical Review E 83, 016305 (2011).

[18] L. M. Pismen, Y. Pomeau, Disjoining potential and spreading of thin liquid layers in the diffuse-interface model coupled to hydrodynamics, Physical Review E 62, 2480 (2000).

[19] U. Thiele, M. Mertig, W. Pompe, Dewetting of an Evaporating Thin Liquid Film : Heterogeneous Nucleation and Surface Instability, Phys. Rev. Lett. 80, 2869 (1998).

[20] U. Thiele, M.G. Velarde, K. Neuffer, Y. Pomeau, Film rupture in the diffuse interface model coupled to hydrodynamics, Physical Review 5 64, 031602 (2001).

[21] U. Thiele, M.G. Velarde, K. Neuffer, Y. Pomeau, On the importance of nucleation solutions for the rupture of thin liquid films, Colloids Surfaces A 206, 135 (2002).

[22] B. Dai, L. Gary Leal, A. Redondo, Disjoining pressure for nonuniform thin films, Physical Review E 78, 061602 (2008).

[23] L.M. Hocking, The influence of intermolecular forces on thin fluid layers, Physics of fluids A : Fluid Dynamics 5, 793 (1993).

[24] C. Huh, L.E. Scriven, Hydrodynamical model of steady movement of a liquid/solid/fluid contact line, J. Colloid Interface Sci. 35, 85-101 (1971).

[25] H.K. Moffatt, Viscous and resistive eddies near a sharp corner, J. Fluid Mech. 18, 1-17 (1964).

[26] A.L. Bertozzi, M.P. Brenner, Linear stability and transient growth in driven contact lines, Physics of Fluids 9, 530 (1997).

[27] M. Roux, Modèles de fronts pour films minces, Thèse de doctorat, INSA Toulouse (2012).

[28] L.H. Tanner, The spreading of silicone oil drops on horizontal surfaces, J. Phys. D 12, 1473 (1979).

[29] A. Zosel, Studies of the wetting kinetics of liquid drops on solid surfaces, Colloid Polym. Sci. 271, 680 (1993).

[30] J.A. Diez, L. Kondic, On the breakup of fluid films of finite and infinite extent, Physics of Fluids 19, 072107 (2007).

[31] H.S. Kheshgi, L.E. Scriven, Dewetting : Nucleation and Growth of dry regions, Chem. Eng. Sci. 46, 519 (1991).

[32] G. Reiter, Dewetting of Thin Polymer Films, Phys. Rev. Lett. 68, 75 (1992).

[33] R. Seemann, K. Jacobs, S. Herminghaus, Dewetting Patterns and Molecular Forces : A Reconciliation, Phys. Rev. Lett. 86, 5534 (2001).

[34] O. Baumchen, M. Lessel, R. Fetzer, R. Seemann, K. Jacobs Sliding fluids : Dewetting experiments reveal the solid/liquid boundary condition, J. Phys. Conf. Ser. 216, 012002 (2010).

[35] K. Zhang, An experimental investigation on the surface water transport process over an airfoil by using a digital image projection technique, Exp Fluids 56, 173 (2015).

[36] P. Noble, JP Vila, Stability theory for difference approximations of some dispersive shallow water equations and application to thin film flows, SIAM J. Numer. Anal., 52(6), 2770-2791 (2014)